We are IntechOpen, the world's leading publisher of Open Access books Built by scientists, for scientists

4,800
Open access books available

122,000
International authors and editors

135M
Downloads

Our authors are among the

154
Countries delivered to

TOP 1%
most cited scientists

12.2%
Contributors from top 500 universities

WEB OF SCIENCE™

Selection of our books indexed in the Book Citation Index in Web of Science™ Core Collection (BKCI)

Interested in publishing with us?
Contact book.department@intechopen.com

Numbers displayed above are based on latest data collected.
For more information visit www.intechopen.com

16

Ultrashort, Strongly Focused Laser Pulses in Free Space

Alexandre April
Centre d'optique, photonique et laser, Université Laval
Québec, Canada

1. Introduction

Technological advances in ultrafast optics now allow the generation of laser pulses whose duration is as short as a few optical cycles of the electric field; furthermore, these pulses can be focused to a spot size comparable to the wavelength. These strongly focused, ultrashort laser pulses have found applications, for instance, in high-resolution microscopy, particle trapping and electron acceleration. In order to characterize the spatiotemporal behavior of such ultrashort, tightly focused pulses, one needs the expressions of their electromagnetic fields.

Ultrafast nonparaxial pulsed beams must be modeled as exact solutions to Maxwell's equations. Many studies on the propagation of a pulsed beam are based on a scalar paraxial theory, which provides an accurate description of the pulsed beam propagation when the beam divergence angle is small and the beam spot size is much larger than the wavelength for each spectral component. However, the analysis of tightly focused laser beams requires expressions of optical beams that extend beyond the paraxial approximation. Moreover, the vector nature of light cannot be neglected to properly describe tightly focused beams. Also, the appropriate spectrum amplitude must be employed in order to model ultrashort pulses.

Many authors have proposed expressions for the electromagnetic fields of laser pulsed beams, but most of these models are incomplete. For example, Wang and co-workers presented scalar paraxial pulsed Gaussian beams that have a Gaussian spectrum (Wang *et al.*, 1997), but their expressions are not suitable to describe ultrashort pulses, as reported by Porras (Porras, 1998). Caron and Potvliege suggested forms of spectra, which are appropriate to characterize pulses of very small duration, but the expressions for their vectorial nonparaxial ultrashort pulses are written in terms of numerically calculated angular spectra (Caron & Potvliege, 1999). Lin *et al.* presented closed-form expressions for subcycle pulsed focused vector beams that are exact solutions to Maxwell's equations obtained in the context of the so-called complex-source point method, but they used an unsuitable Gaussian spectrum (Lin *et al.*, 2006). Recently, an der Brügge and Pukhov have provided solutions for ultrashort focused electromagnetic pulses found with a more appropriate spectral amplitude, but the expressions hold true only in the paraxial regime (an der Brügge & Pukhov, 2009).

The aim of this chapter is to provide a simple and complete strategy to correctly model strongly focused, ultrashort laser pulses. Three main tools are employed to find the expressions for the fields of such pulsed beam. First, the Hertz potential method is used in

order to efficiently obtain the spatiotemporal expressions for the electromagnetic fields that rigorously satisfy Maxwell's four equations. Then, the complex source/sink model is exploited to determine an exact solution to the Helmholtz equation that describes a physically realizable nonparaxial beam that generalizes the standard Gaussian beam. Finally, the so-called Poisson-like spectrum is employed to characterize ultrashort pulses whose duration could be as short as one optical cycle. The combination of these three main ingredients leads to closed-form expressions that accurately describe the electromagnetic fields of laser pulsed beams in free space.

This chapter is divided as follows. In Section 2, the traditional theories used to characterize laser pulsed beams are briefly exposed. In Section 3, the Hertz potential method, the complex-source/sink model, and the Poisson-like spectrum are introduced. In Section 4, the method presented in this chapter is applied to selected types of laser pulses. Finally, in Section 5, one of these special case is investigated in detail to shed light on features related to the propagation of tightly focused, ultrashort pulsed beams.

2. The traditional theories of pulsed beams

Well-established theories for laser pulsed beams are available, but many of them remain accurate only in some specific regimes. A number of authors have treated the propagation of ultrashort, nonparaxial laser pulses with a scalar analysis, although the vector nature of light cannot be ignored for strongly focused beams (Porras, 1998; Saari, 2001; Lu *et al*., 2003). Some authors have given solutions for ultrashort pulsed beams within the paraxial approximation, whose validity may be questioned for pulses with spectral distributions extending to very low frequencies (Feng & Winful, 2000; an der Brügge & Pukhov, 2009). Others have presented solutions for ultrashort nonparaxial electromagnetic pulsed beams having a Gaussian spectrum, which is not suitable to describe such pulses (Wang *et al*., 1997; Lin *et al*., 2006). In fact, the scalar treatment, the paraxial approximation and the Gaussian spectrum are not adequate to model ultrashort, tightly focused pulsed beams. In this section, the shortcomings encountered with these traditional approaches are explored.

2.1 The scalar wave function

To theoretically describe the spatiotemporal behavior of ultrashort, nonparaxial pulses, one needs expressions of their electromagnetic fields that are exact solutions of the wave equation. The electric field $\mathbf{E}(\mathbf{r},t)$ and the magnetic field $\mathbf{H}(\mathbf{r},t)$ of a laser pulse must satisfy Maxwell's equations. In differential form, these fundamental equations in free space are given in Table 1.

Faraday's law	Ampère-Maxwell law	Gauss's law for **E**	Gauss's law for **H**
$\nabla \times \mathbf{E} = -\mu_0 \frac{\partial \mathbf{H}}{\partial t}$	$\nabla \times \mathbf{H} = \varepsilon_0 \frac{\partial \mathbf{E}}{\partial t}$	$\nabla \bullet \mathbf{E} = 0$	$\nabla \bullet \mathbf{H} = 0$

Table 1. Maxwell's equations in free space.

Here, μ_0 and ε_0 are the permeability and the permittivity of free space, respectively. The principle of duality applies in free space: the substitutions $\mathbf{E} \to \eta_0 \mathbf{H}$ and $\mathbf{H} \to -\mathbf{E}/\eta_0$, where $\eta_0 = (\mu_0/\varepsilon_0)^{1/2}$ is the intrinsic impedance of free space, leave Maxwell's four equations unchanged. From Maxwell's equations, one can obtain the wave equations in free space for the electric and the magnetic fields:

$$\nabla^2\mathbf{E} - \frac{1}{c^2}\frac{\partial^2\mathbf{E}}{\partial t^2} = \mathbf{0}\,, \tag{1a}$$

$$\nabla^2\mathbf{H} - \frac{1}{c^2}\frac{\partial^2\mathbf{H}}{\partial t^2} = \mathbf{0}\,, \tag{1b}$$

where $c = (\mu_0\varepsilon_0)^{1/2}$ is the speed of light in free space. Thus, each Cartesian component of the electric and the magnetic fields must satisfy the scalar wave equation.

The electromagnetic fields can be analyzed in the frequency domain by taking the Fourier transform of Eqs. (1a) and (1b): the temporal derivatives $\partial/\partial t$ are then converted to $j\omega$, where $\omega = kc$ is the angular frequency of the spectral component and k is its wave number. The Fourier transforms of the electric and the magnetic fields, denoted by $\tilde{\mathbf{E}}$ and $\tilde{\mathbf{H}}$ respectively, must satisfy the vector Helmholtz equations $\nabla^2\tilde{\mathbf{E}} + k^2\tilde{\mathbf{E}} = \mathbf{0}$ and $\nabla^2\tilde{\mathbf{H}} + k^2\tilde{\mathbf{H}} = \mathbf{0}$. It is often assumed that a laser beam is a transverse electromagnetic (TEM) beam, that is, the electric and the magnetic fields are always transverse to the propagation axis, which is the z-axis in this chapter. However, the only true TEM waves in free space are infinitely extended fields. For example, consider a x-polarized beam for which the y-component E_y of its electric field is zero; the x-component E_x of its electric field satisfies the scalar wave equation $\nabla^2 E_x - c^{-2}\partial^2 E_x/\partial t^2 = 0$, from which a solution for E_x may be found. One can estimate the longitudinal electric field component of this x-polarized optical beam by applying Gauss's law for $\mathbf{E}$ to such a beam, giving an expression for the z-component E_z of the beam:

$$E_z = -\int \frac{\partial E_x}{\partial x}\mathrm{d}z\,. \tag{2}$$

Since an optical beam has a finite spatial extent in the plane transverse to the direction of propagation, the component E_x must depend on the transverse coordinate x and, therefore, E_z must be different from zero. Thus, even if it only exhibits a small beam divergence angle, an optical beam always has a field component that is polarized in the direction of the propagation axis. The same argument applies to the magnetic field. In some cases, the strength of the longitudinal component of the fields of a tightly focused laser beam can even exceed the strength of its transverse components. As a result, in order to accurately characterize laser beams or pulses, a vectorial description of their electromagnetic fields is needed and will be discussed in Section 3.1.

2.2 The paraxial approximation

In many applications in optics, the light beam propagates along a certain direction (here, along the z-axis) and spreads out slowly in the transverse direction. When the beam divergence angle is small, the beam is said to be paraxial. Specifically, the electric field of a paraxial beam in the frequency domain is a plane wave $\exp(-jkz)$ of wavelength $\lambda = 2\pi/k$ modulated by a complex envelope that is assumed to be approximately constant within a neighborhood of size λ. The phasor of the x-component of a paraxial beam is therefore written as $\tilde{E}_x = \tilde{A}\exp(-jkz)$, where $\tilde{A}$ is the complex envelope that is a slowly varying function of position. The complex enveloppe must satisfy the paraxial Helmholtz equation (Siegman, 1986):

$$\frac{\partial^2\tilde{A}}{\partial x^2} + \frac{\partial^2\tilde{A}}{\partial y^2} - 2jk\frac{\partial\tilde{A}}{\partial z} = 0\,, \tag{3}$$

provided that the condition $\left|\partial^2 \tilde{A}/\partial z^2\right| << \left|2k\partial\tilde{A}/\partial z\right|$ is verified. This condition is called the slowly varying envelope approximation or simply the paraxial approximation. When it applies, the use of this approximation considerably simplifies the analysis of optical beams in many applications.

To model a laser beam, the Gaussian beam is often used. The phasor of the paraxial Gaussian beam, whose envelope is a solution to the paraxial Helmholtz equation, is (Siegman, 1986)

$$\tilde{u}(\mathbf{r},\omega) = F(\omega)\frac{jz_R}{\tilde{q}(z)}\exp\left[-jk\left(\frac{r^2}{2\tilde{q}(z)}+z\right)\right], \tag{4}$$

where $F(\omega)$ is an arbitrary function of the frequency ω only, r and z are the radial and the longitudinal coordinates, respectively, $\tilde{q}(z) = z + jz_R$ is the complex radius of curvature, $z_R = \frac{1}{2}kw_0^2$ is the Rayleigh range, and w_0 is the waist spot size of the beam. The beam divergence angle is given by $\delta \equiv \arctan\left(w_o/z_R\right)$.

The envelope of the Gaussian beam is one solution of the paraxial Helmholtz equation among the infinite number of solutions of this differential equation. Well-known solutions are the envelopes of the higher-order Gaussian modes which include standard and elegant Hermite–Gaussian or Laguerre–Gaussian beams. The elegant beams were introduced by Siegman and they differ from the standard beams because the former contain polynomials with a complex argument, whereas in the latter the argument is real (Siegman, 1986). Physically, the standard beams constitute the natural modes of a stable laser resonator with mirrors having uniform reflectivity, while the elegant beams describe modes generated by a laser resonant cavity that includes soft Gaussian apertures. Both modes form an eigenfunction basis to the paraxial Helmholtz equation. While the Hermite–Gaussian modes are adequate to describe optical beams with rectangular geometry, the Laguerre–Gaussian modes are more appropriate to describe beams with cylindrical symmetry. The phasor of the paraxial elegant Laguerre–Gaussian beam is (April, 2008a)

$$\tilde{u}^e_{p,m}(\mathbf{r},\omega) = F(\omega)\left(\frac{jz_R}{\tilde{q}(z)}\right)^{p+m+1}\frac{r^m}{w_o^m}L_p^m\left(\frac{jkr^2}{2\tilde{q}(z)}\right)\exp\left[-jk\left(\frac{r^2}{2\tilde{q}(z)}+z\right)\right]\cos(m\phi), \tag{5}$$

where p = 0,1,2,… is the radial mode number, m = 0,1,2,… is the angular mode number, $L_p^m(\cdot)$ is the associated Laguerre polynomial, and ϕ is the azimuthal angle. Superscript "e" in solutions $\tilde{u}^e_{p,m}$ stands for even modes, with the even function $\cos(m\phi)$ for the azimuthal dependence. Odd modes $\tilde{u}^o_{p,m}$ are obtained by replacing $\cos(m\phi)$ in Eq. (5) by $\sin(m\phi)$. If $p = m = 0$, then Eq. (5) reduces to Eq. (4), i.e. $\tilde{u}^e_{0,0}(\mathbf{r},\omega) = \tilde{u}(\mathbf{r},\omega)$. Both Eqs. (4) and (5) are accurate if the paraxial approximation holds, i.e. when the waist spot size w_0 is not too small with respect to the wavelength λ or more precisely when $w_0 >> \lambda/(\pi\sqrt{2})$.

If the envelope is not a slowly varying function of position, the paraxial approximation does not apply. In fact, when the waist spot size of an optical beam is smaller than the wavelength, the beam is said to be nonparaxial. Moreover, some spectral components of an ultrashort pulsed beam can be considered paraxial while others in the same pulse are nonparaxial. In brief, to accurately describe ultrashort strongly focused pulses, the nonparaxial effects have to be taken into account; thus, exact solutions to the wave equation for their electromagnetic fields are required and will be provided in Section 3.2.

2.3 The Gaussian spectrum

In many cases, it is convenient to use a Gaussian spectrum to model a physical laser pulse. However, for an ultrashort pulsed beam, which has a very broad spectrum, the Gaussian spectrum is no longer appropriate, because the spectral content cannot physically extend in negative frequencies (Caron & Potvliege, 1999). In fact, while it accurately describes the beamlike behavior near the optical axis, the amplitude distribution becomes boundless for large values of the transverse coordinate.

In order to briefly investigate this shortcoming, consider a paraxial Gaussian pulse that has the following Gaussian spectrum:

$$F(\omega) = T\sqrt{\pi}\exp\left[-\tfrac{1}{4}T^2\left(\omega-\omega_o\right)^2 + j\phi_o\right], \tag{6}$$

where T is the duration of the pulse, ω_o is the frequency of the carrier wave, and ϕ_o is a constant phase. The analytic signal $u(\mathbf{r},t)$ of the Gaussian pulse in the temporal domain is obtained by taking the inverse Fourier transform of the function $\tilde{u}(\mathbf{r},\omega)$ given by Eq. (4), i.e.

$$u(\mathbf{r},t) = \frac{1}{2\pi}\int_{-\infty}^{\infty}\tilde{u}(\mathbf{r},\omega)\exp(j\omega t)\mathrm{d}\omega\,. \tag{7}$$

When Eqs. (4) and (6) are substituted in Eq. (7), an integral over ω remains to be solved; the dependence on ω in $\tilde{u}(\mathbf{r},\omega)$ comes from $F(\omega)$ and k (because $k=\omega/c$).

We now consider a so-called isodiffracting pulse (Wang *et al.*, 1997; Caron & Potvliege, 1999; Feng & Winful, 2000). For this type of pulse, all the frequency components have the same Rayleigh range z_R. It may be argued that a mode-locked laser produces isodiffracting pulses, because the Rayleigh range of the generated optical beam is determined by the geometry of the laser cavity only and is thus independent of the frequency ω. In fact, many authors have pointed out that isodiffracting pulses are natural spatiotemporal modes of a curved mirror laser cavity. For isodiffracting pulses, the complex radius of curvature $\tilde{q}(z)$ is frequency independent and, thus, the inverse Fourier transform of Eq. (7) can be easily carried out:

$$u(r,z,t) = \frac{jz_R}{\tilde{q}(z)}\exp\left[j(\omega_o t+\phi_o) - \frac{1}{T^2}\left(t-\frac{z}{c}-\frac{r^2}{2c\tilde{q}(z)}\right)^2 - jk_o\left(z+\frac{r^2}{2\tilde{q}(z)}\right)\right]. \tag{8}$$

Here, $k_o=\omega_o/c$ is the wave number of the carrier wave and c is the speed of light in free space. The physical pulsed beam is the real part of Eq. (8). This equation shows that there is spatiotemporal coupling, i.e. there exists a coupling among the beam parameters in space and time. In fact, the spatial coordinates are involved in the temporal shape of the pulse, whereas the duration of the pulse is involved in the spatial distribution of the pulsed beam.

The pulsed beam modeled by Eq. (8) is not a well-behaved solution: the amplitude profile is boundless for large values of the transverse coordinate r. As a consequence, the energy carried by the beam is infinite. To show this drawback explicitly, consider Eq. (8) when the pulse is in the beam waist ($z = t = 0$):

$$u(r,0,0) = \exp\left[\frac{r^4}{(2cTz_R)^2} - \frac{k_o r^2}{2z_R} + j\phi_o\right]. \tag{9}$$

This amplitude profile grows as $\exp(r^4)$ for large values of r – more precisely, for $r >> T(2\omega_o z_R c)^{1/2}$. According to this condition, the amplitude growth is not encountered if the pulse is a pulsed plane wave (for which $z_R \to \infty$) or if the Gaussian spectrum is narrow enough (i.e. if $\omega_o T >> 1$). The reason of this unphysical growth is a consequence of the existence of negative frequencies in the spectral content of the pulsed beam. In fact, the Gaussian spectrum $F(\omega)$ does not vanish for $\omega < 0$, and the amplitudes of the spectral components with negative frequency, however small they are, grow exponentially for sufficently large values of the transverse coordinate. It must be concluded that a Gaussian spectrum is not suitable to characterize arbitrarily short laser pulses. A suitable spectrum will be introduced in Section 3.3.

3. The three tools to model nonparaxial, ultrashort laser pulses

To find adequate expressions that correctly characterize the fields of ultrashort nonparaxial electromagnetic pulses in all regimes, three main tools are used. First, to obtain all the electromagnetic fields components that satisfy Maxwell's equations exactly, the Hertz potential method is employed. Second, to solve the Helmholtz equation rigorously, the complex-source/sink method is exploited. Third, to model ultrafast pulses whose duration could be as short as one optical cycle of the electric field, a Poisson-like spectrum is used.

3.1 The Hertz potential method

As mentioned in Section 2, when the beam divergence angle becomes sufficently large, not only the paraxial approximation does not hold, but a scalar treatment is no longer adequate. To accurately desbribe a strongly focused beam, the phasors of its electromagnetic fields must be exact solutions to Maxwell's equations. Many authors have proposed expressions for the electric field of an optical beam that is a rigorous solution to Maxwell's equations. Richards and Wolf developed an integral representation of the electric field of a tightly focused beam (Richards & Wolf, 1959); nevertheless, the integrals have to be solved numerically in general. Another method, developed by Lax, Louisell and McKnight, consists in adding corrections to the phasor of the paraxial beam (Lax *et al*., 1975). The resulting phasor is therefore expressed as a troncated power series; the larger the number of terms is, the more accurate is the expression. According to the methods of Richards and Wolf as well as of Lax *et al*., the vector wave equation is solved for the electric field. This approach is rather complicated since the electric field of an optical beam generally has three nonzero components. The Hertz potential method allows to solve Maxwell's equations in a more efficient way.

The physical fields that have to be determined, for a given laser pulse, are the electric field $\mathbf{E}(\mathbf{r},t)$ and the magnetic field $\mathbf{H}(\mathbf{r},t)$. However, it is often useful to introduce the vector magnetic potential $\mathbf{A}(\mathbf{r},t)$ and the electric potential $V(\mathbf{r},t)$, which are defined by $\mathbf{H} \equiv (1/\mu_0)\nabla \times \mathbf{A}$ and $\mathbf{E} \equiv -\nabla V - \partial \mathbf{A}/\partial t$. Because a vector is entirely defined only if its divergence and its curl are specified, the divergence of the vector magnetic potential must be defined and it is usually determined with the Lorenz condition for potentials: $c^2 \nabla \bullet \mathbf{A} + \partial V/\partial t = 0$, where c is the speed of light in vacuum. With the Lorenz condition, the vector magnetic potential and the electric potential both satisfy the wave equation in free space. The vector magnetic potential and the electric potential are introduced in order to simplify the computation of electromagnetic fields; often, potentials are easily computed and then electromagnetic fields are directly deduced from the definitions of these potentials.

The Hertz potential method is a powerful tool that can be used to determine the spatiotemporal expressions for the electromagnetic fields of pulsed beams. The electric and magnetic Hertz potentials, $\mathbf{\Pi}_e$ and $\mathbf{\Pi}_m$ respectively, are defined in terms of the electromagnetic potentials: $V \equiv -\nabla \bullet \mathbf{\Pi}_e$ and $\mathbf{A} \equiv (1/c^2)\partial \mathbf{\Pi}_e / \partial t + \mu_0 \nabla \times \mathbf{\Pi}_m$. This particular choice for the Hertz potentials is such that the Lorenz condition is identically verified, since the divergence operator and the temporal derivative commute and since the divergence of a curl vanishes. The Hertz potentials may be seen as "super-potentials" in the sense that they are vector potentials from which other potentials can be obtained. Similarly to the electromagnetic fields and the electromagnetic potentials, the Hertz potentials are also chosen to satisfy the wave equation in free space:

$$\nabla^2 \mathbf{\Pi}_e - \frac{1}{c^2}\frac{\partial^2 \mathbf{\Pi}_e}{\partial t^2} = \mathbf{0}\,, \tag{10a}$$

$$\nabla^2 \mathbf{\Pi}_m - \frac{1}{c^2}\frac{\partial^2 \mathbf{\Pi}_m}{\partial t^2} = \mathbf{0}\,. \tag{10b}$$

If Eqs. (10a) and (10b) are satisfied, then the electric field $\mathbf{E}(\mathbf{r},t)$ and the magnetic field $\mathbf{H}(\mathbf{r},t)$ may be obtained with the following relationships (Sheppard, 2000):

$$\mathbf{E} = \nabla \times \nabla \times \mathbf{\Pi}_e - \mu_0 \frac{\partial}{\partial t}\nabla \times \mathbf{\Pi}_m \tag{11a}$$

$$\mathbf{H} = \nabla \times \nabla \times \mathbf{\Pi}_m + \varepsilon_0 \frac{\partial}{\partial t}\nabla \times \mathbf{\Pi}_e \tag{11b}$$

It can be verified by straightforward calculations that Eqs. (11a) and (11b) satisfy identically Maxwell's four equations in free space if $\mathbf{\Pi}_e$ and $\mathbf{\Pi}_m$ are both solutions of the vector wave equation. Thus, if the Hertz potentials are known for a given pulsed beam, then the electromagnetic fields are deduced by applying Eqs. (11a) and (11b).

The Hertz potential method consists in assuming that the Hertz potentials are linearly polarized. Accordingly, the nonzero Cartesian component of $\mathbf{\Pi}_e$ and $\mathbf{\Pi}_m$ obeys a scalar wave equation whereas the electromagnetic fields still have to obey a vector wave equation, since all the components of the fields are nonzero in general. It can be seen, therefore, that working with the Hertz potentials has the advantage of simplifying the determination of a solution to the wave equation. In fact, dealing directly with the electric and the magnetic fields, it is necessary to solve a vector wave equation for the fields instead of a scalar wave equation for the Hertz potentials.

The appropriate choice of the nonzero components of the Hertz potentials depends on the state of polarisation of the given pulsed beam. Among others, three states of polarization can be easily generated with the Hertz potential method: transverse magnetic (TM), transverse electric (TE), and linearly polarized (LP) beams. TM beams may be obtained with an electric Hertz potential oriented along the propagation axis ($\mathbf{\Pi}_e = \hat{\mathbf{a}}_z \Psi(\mathbf{r},t)$ and $\mathbf{\Pi}_m = \mathbf{0}$, where $\Psi(\mathbf{r},t)$ is a scalar function with V · m units), whereas TE beams may be obtained with a magnetic Hertz potential oriented along the z-axis ($\mathbf{\Pi}_e = \mathbf{0}$ and $\mathbf{\Pi}_m = \hat{\mathbf{a}}_z \eta_0^{-1} \Psi(\mathbf{r},t)$, where η_0 is the intrinsic impedance of free space). Also, a linearly polarized beam can be produced by a combination of an electric dipole and a magnetic dipole, oriented along the x- and the y-axes, respectively, or in other words by setting $\mathbf{\Pi}_e = \hat{\mathbf{a}}_x \Psi(\mathbf{r},t)$ and $\mathbf{\Pi}_m = \hat{\mathbf{a}}_y \eta_0^{-1} \Psi(\mathbf{r},t)$.

Hence, we are looking for a rigorous solution to the scalar wave equation for the nonzero Cartesian component $\Psi(\mathbf{r},t)$ of the Hertz potentials.

3.2 The complex source/sink model

The methods from Richards and Wolf and from Lax *et al*. previously mentioned give solutions to the wave equation for the electric field of an optical beam. The former leads to an integral representation of the electric field while the latter gives an infinite-series expansion of the field. However, integral representations or series expansion of an optical beam become computationally onerous or increasingly inaccurate as the beam divergence angle grows. Hence, closed-form solutions for the electromagnetic fields of a nonparaxial beam would be interesting to avoid such an inconvenience. First, the so-called complex point-source method is introduced; second, the confocal parameter that characterizes the beam divergence is clearly defined; third, the complex source/sink model which does not exhibit the shortcomings of the complex point-source method is explained; finally, the nonparaxial higher-order beams are presented.

The complex point-source model

The complex point-source method is a simple approach to obtain a rigorous solution to the Helmholtz equation, expressed in a simple closed form, that describes a nonparaxial beam. Deschamps has been the first to introduce the complex source-point method, which consists in assuming that the beam is generated by a source located at an imaginary distance along the propagation axis (Deschamp, 1971). Mathematically, it means that the longitudinal coordinate of the phasor of the wave is replaced by a complex quantity whose imaginary part is closely related to the beam divergence angle. The complex source-point method turns out to be a useful technique to convert a spherical wave into a nonparaxial Gaussian beam.

Couture and Bélanger have shown that, in the context of the perturbative method of Lax *et al*., the sum of all the corrections to the paraxial Gaussian beam transforms the Gaussian beam into the complex source-point spherical wave (Couture & Bélanger, 1981). Thus, the complex source-point method is equivalent to the approach of Lax *et al*., provided that the boundary condition is such that the corrections are zero along the optical axis of the beam. The complex source-point method allows to analytically write the phasor of a nonparaxial optical beam in a closed form, without having to deal explicitly with a series expansion.

It is well known that the phasor of the paraxial Gaussian beam [Eq. (4)] can be formally obtained if it is assumed that it consists in a paraxial spherical wave (a parabolic wave) emitted by a point source positioned at the imaginary distance $-jz_R$ along the propagation axis, where z_R is the Rayleigh range of the beam (Siegman, 1986). With a similar approach applied to the phasor of a nonparaxial spherical wave, one can obtain the phasor of a nonparaxial Gaussian beam.

The components of the Hertz potentials are now considered in the spectral domain. The Fourier transform of the function $\Psi(\mathbf{r},t)$, denoted by $\tilde{\Psi}(\mathbf{r},\omega)$, must then satisfy the scalar Helmholtz equation $\nabla^2\tilde{\Psi}+k^2\tilde{\Psi}=0$, where $k=\omega/c$ is the wave number of the spectral component of angular frequency ω (Fig. 1). The phasor of the spherical wave is a rigorous solution to the scalar Helmholtz equation; it is expressed as $\exp(-jkR)/R$, where $R=[x^2+y^2+(z-z_s)^2]^{1/2}$ is the spherical radius of curvature of the wave and z_s is the axial location of the point source. We now convert z_s into a pure imaginary number, i.e. $z_s=-ja$, where a is real constant called the confocal parameter (Sheppard & Saghafi, 1999a). The

complex spherical radius is therefore $\tilde{R} = [r^2 + (z + ja)^2]^{1/2}$, where $r = (x^2 + y^2)^{1/2}$ is the transverse coordinate. The phasor of the nonparaxial Gaussian beam is then

$$\tilde{\Psi}^{+}(\mathbf{r}, \omega) = \exp(-ka)\exp(-jk\tilde{R})/\tilde{R}, \tag{12}$$

where exp(–*ka*) is a standard normalization constant, which ensures the continuity of the solution between the paraxial and the nonparaxial regimes. The superscript "+" recalls that the beam is diverging from the origin. The phasor $\tilde{\Psi}^{-}(\mathbf{r}, \omega) = \exp(-ka)\exp(+jk\tilde{R})/\tilde{R}$ represents a beam that is converging toward the origin.

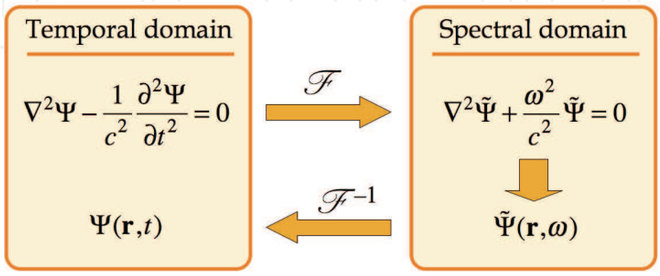

Fig. 1. By a Fourier transformation, the wave equation for the Hertz potential is converted into the Helmholtz equation, which is solved in the spectral domain; thanks to an inverse Fourier transformation, the phasor obtained is then converted into an exact spatiotemporal solution to the wave equation for the component of the Hertz potential.

The confocal parameter

The phasor of the nonparaxial Gaussian beam obtained with the help of the complex source-point method depends on the parameter *a*, which is the confocal parameter of the oblate spheroidal coordinates (Landesman & Barrett, 1988). In fact, it turns out that the oblate spheroidal coordinates (ξ, η, ϕ) are the ones in which it is natural to express the phasor of the nonparaxial Gaussian beam. Consider a system of mutually orthogonal, confocal ellipses and hyperbolas in the sense that the ellipses and the hyperbolas share the same foci and intersect at right angles. The distance between the origin and each focus is *a*. The surfaces of the oblate spheroidal coordinate system are formed by rotating the system of confocal ellipses and hyperbolas about the minor axis of the ellipse (Fig. 2). The rotation axis is *z* and the resulting focus is a ring of radius *a* in the *x*-*y* plane.

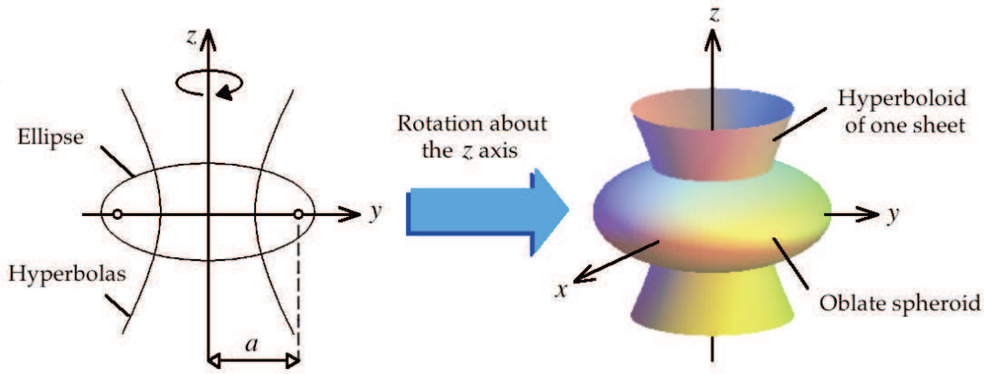

Fig. 2. The surfaces of the oblate spheroidal coordinate system are formed by rotating a system of confocal ellipses and hyperbolas about the *z*-axis.

The Cartesian coordinates (x,y,z) and the oblate spheroidal coordinates (ξ,η,ϕ) are related by the parametric equations $x = a[(1+\xi^2)(1-\eta^2)]^{1/2}\cos\phi$, $y = a[(1+\xi^2)(1-\eta^2)]^{1/2}\sin\phi$, and $z = a\xi\eta$, where $\xi \geq 0$, $-1 \leq \eta \leq 1$, and $0 \leq \phi \leq 2\pi$, and where a is the confocal parameter.
The real and imaginary parts of the complex spherical radius $\tilde{R}$ can be easily expressed in terms of the oblate spheroidal coordinates. Substituting the parametric equations relating the Cartesian coordinates and the oblate spheroidal coordinates in $\tilde{R} = [x^2 + y^2 + (z + ja)^2]^{1/2}$ yields $\tilde{R} = a(\xi + j\eta)$. The real part of $\tilde{R}$ is $a\xi$ while its imaginary part is $a\eta$. It is therefore convenient to express the coordinates ξ and η in terms of the Cartesian coordinates [Berardi, 2004]:

$$\xi = \frac{1}{\sqrt{2}a}\left\{\left(R^2 - a^2\right) + \left[\left(R^2 - a^2\right)^2 + 4a^2z^2\right]^{1/2}\right\}^{1/2}, \tag{13a}$$

$$\eta = \sqrt{2}z\left\{\left(R^2 - a^2\right) + \left[\left(R^2 - a^2\right)^2 + 4a^2z^2\right]^{1/2}\right\}^{-1/2}, \tag{13b}$$

where $R^2 = x^2 + y^2 + z^2$. The parameter *a*, which characterizes the divergence of the beam, is related to the Rayleigh range of the beam. The distance between the origin and the foci of the hyperbolas is *a* whereas the angle between the *z*-axis and the asymptotes is δ (Fig. 3).

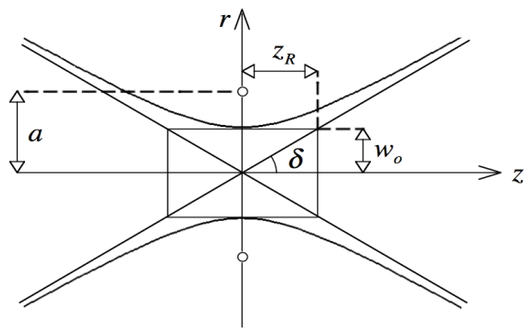

Fig. 3. The waist spot size, the Rayleigh range and the divergence angle of the nonparaxial beam are characteristics of the hyperboloid that defines the oblate spheroidal coordinates.

The waist spot size w_o is defined as the length of the semi-major axis of the hyperbola while the Rayleigh range is defined by the length of the semi-minor axis (Fig. 3). From the geometry of the hyperbola, the Rayleigh range is given by $z_R \equiv \frac{1}{2}kw_o^2 = (a^2 - w_o^2)^{1/2}$ (Rodríguez-Morales & Chávez-Cerda, 2004). The last equality provides a quadratic equation in w_o^2. Solving this equation for w_o^2 results in $w_o^2 = (2/k^2)\{[1+(ka)^2]^{1/2} - 1\}$. Consequently, for a given wave number $k = 2\pi/\lambda$, the confocal parameter can be written in terms of the waist spot size w_o, the Rayleigh range $z_R = \frac{1}{2}kw_o^2$, or the beam divergence angle $\delta \equiv \arctan(w_o/z_R)$. All the relationships between these parameters are listed in Table 2.
Large values of ka refer to the paraxial regime and small values of ka correspond to the nonparaxial regime. The phasor of the Gaussian beam tends to the uniform plane wave if ka is very large, whereas it becomes the phasor of the spherical wave if $ka = 0$. The threshold between the paraxial and the nonparaxial regimes cannot be clearly defined. Nonetheless, it is usually accepted that the beam divergence angle of a paraxial beam must

not exceed 30°. Therefore, as a rule of thumb, the paraxial approximation can be used as far as ka is greater than 7 (Rodrígez-Morales & Chávez-Cerda, 2004). Note that, in the limit $ka >> 1$, the confocal parameter a tends to the Rayleigh range z_R.

Waist spot size w_o	$w_o = \left(\frac{2z_R}{k}\right)^{1/2}$	$w_o = \frac{2}{k\tan\delta}$	$w_o = \frac{\sqrt{2}}{k}\left\{\left[1+(ka)^2\right]^{1/2}-1\right\}^{1/2}$
Rayleigh range z_R	$z_R = \frac{1}{2}kw_o^2$	$z_R = \frac{2}{k\tan^2\delta}$	$z_R = \frac{\left[1+(ka)^2\right]^{1/2}-1}{k}$
Beam divergence angle δ	$\tan\delta = \frac{2}{kw_o}$	$\tan\delta = \left(\frac{2}{kz_R}\right)^{1/2}$	$\cos\delta = \frac{\left[1+(ka)^2\right]^{1/2}-1}{ka}$
Confocal parameter a	$a = \frac{2}{k\sin\delta\tan\delta}$	$a = z_R\left(1+\frac{2}{kz_R}\right)^{1/2}$	$a = w_o\left[1+(\frac{1}{2}kw_o)^2\right]^{1/2}$

Table 2. Relationships between the waist spot size, the Rayleigh range, the beam divergence angle, and the confocal parameter.

The complex source/sink model

The complex source/sink model is a simple approach to find an exact solution to the Helmholtz equation that describes a physically realizable nonparaxial beam (Ulanowski & Ludlow, 2000). In fact, it has been pointed out that the phasor of the nonparaxial Gaussian beam as defined by Eq. (12) has two shortcomings: an axial discontinuity and a circular singularity of radius a occur in the plane of the beam waist (Fig 4a). On the one hand, the axial discontinuity is due to the choice for the branch of the square root in the complex spherical radius $\tilde{R}$; the height of the discontinuity in the amplitude distribution on the z-axis is $\exp(-2ka)$ and it becomes significant when $ka > 1$. On the other hand, the circular singularity can be explained because Eq. (12) tends to infinity when its denominator vanishes; this happens if $r = a$ in the plane $z = 0$. Nevertheless, such a singularity does not

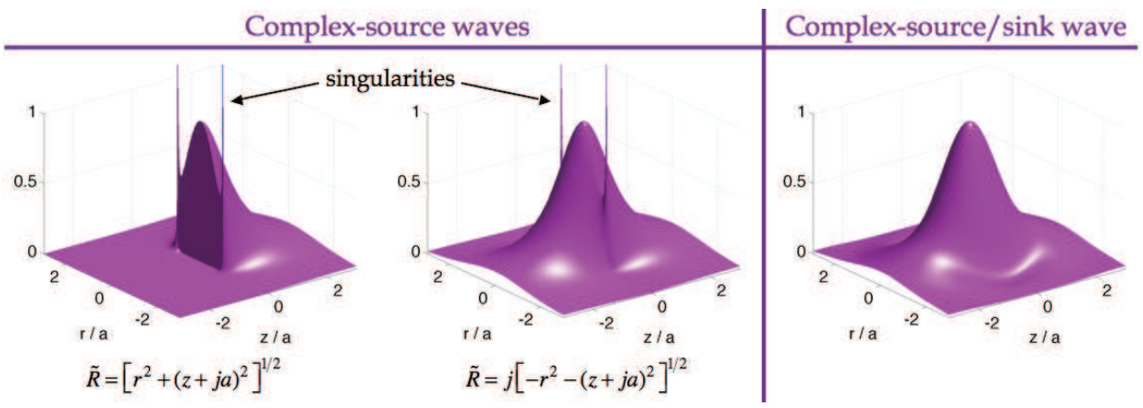

Fig. 4. The square modulus of the phasor of the nonparaxial Gaussian beam near the plane of the beam waist, with ka = 2, (a) has both an axial discontinuity and a singularity with the choice I for the value of the complex spherical radius, (b) exhibits only the singularity with the choice II, and (c) is well-behaved in the context of the complex source/sink model.

have a significant impact on the behavior of the beam if a is large enough with respect to the wavelength λ, i.e. in the paraxial regime ($ka >> 1$).
In the phasor of the nonparaxial Gaussian beam defined by Eq. (12), the choice for the value of the complex spherical radius $\tilde{R}$ is relevant. Two choices can be specified:

[Choice I] $$\tilde{R} = \left[r^2 + \left(z + ja \right)^2 \right]^{1/2}, \tag{14a}$$

[Choice II] $$\tilde{R} = j\left[-r^2 - \left(z + ja \right)^2 \right]^{1/2}. \tag{14b}$$

The value of $\tilde{R}$ for which the real part $a\xi$ is positive corresponds to the choice I, whereas the one for which the imaginary part $a\eta$ is positive is associated to the choice II. In particular, on the optical axis (r = 0), Eq. (14a) reduces to $\tilde{R} = z + ja$ if $z > 0$ and $\tilde{R} = -z - ja$ if $z < 0$ while Eq. (14b) reduces to $\tilde{R} = z + ja$ for all z, considering a as a nonzero positive real number. The choice I in Eq. (12) leads to a wave that radiates outward from the plane of the beam waist (z = 0), while the choice II in Eq. (12) gives a beam traveling from negative z to positive z like a purely traveling beam. Thus, although these two representations are both solutions of the Helmholtz equation, they describe different complex-source waves. The use of the choice II in Eq. (12) removes the axial discontinuity in the phasor of the nonparaxial beam (Fig. 4b). Nonetheless, neither choice of the branch for the square root $\tilde{R}$ in Eq. (12) removes the nonphysical singularity of radius a in the plane of the beam waist. Both complex-source waves in the Figs. 4a and 4b have a singularity at $r = a$ when z = 0, where the square modulus of the phasor tends to infinity. It may be argued that this drawback originates from the description of the field as due to a source (even though it is located at an imaginary coordinate), which is inherently contradictory, since the field is physically source-free in the spatial region under consideration.
Sheppard and Saghafi as well as Ulanowski and Ludlow have shown that the superposition of two counter-propagating beams can remove both the axial discontinuity and the circular singularity (Sheppard & Saghafi, 1998; Ulanowski & Ludlow, 2000). In fact, a singularity-free nonparaxial Gaussian beam is proportional to the superposition $\tilde{\Psi}^{-}(\mathbf{r},\omega) - \tilde{\Psi}^{+}(\mathbf{r},\omega)$. An exact solution to the Helmholtz equation that generalizes the Gaussian beam and that is valid in all space in the nonparaxial regime is therefore

$$\tilde{\Psi}(\mathbf{r},\omega) = \tilde{\Psi}_o F(\omega) \frac{\exp(-ka)}{2j} \left[\frac{\exp(jk\tilde{R})}{\tilde{R}} - \frac{\exp(-jk\tilde{R})}{\tilde{R}} \right] = \tilde{\Psi}_o F(\omega) \exp(-ka) \frac{\sin(k\tilde{R})}{\tilde{R}} \tag{15}$$

where $\tilde{\Psi}_o$ is a constant amplitude and $F(\omega)$ is an arbitrary well-behaved function that represents the spectral amplitude of the pulse. According to the superposition principle, the phasor of Eq. (15) is a rigorous solution of the source-free Helmholtz equation. Eq. (15) is a singularity-free phasor, because it is finite at $\tilde{R} = 0$, and thus describes a physically realizable optical beam (Fig. 4c). Eq. (15) is the same whichever choice is taken for the complex spherical radius $\tilde{R}$. Thus, no great care is needed concerning the specific choice between Eqs. (14a) or (14b) in calculating the phasor of the nonparaxial Gaussian beam of the Eq. (15). Also, it can be shown that the nonparaxial Gaussian beam reduces to the phasor of the paraxial Gaussian beam in the paraxial limit, i.e. Eq. (15) reduces to Eq. (4) when $ka >> 1$ (April, 2008a).

From another point of view, it is seen that the removal of the nonphysical singularity has been accomplished by combining a sink to the source; this leads to what is called the complex source/sink method. In fact, Eq. (15) may be viewed as the superposition of an outgoing beam, produced by the source located at $z_s = -ja$, and an incoming beam, absorbed by the sink placed at the same position. This optical wave, consisting in a superposition of two counter-propagating beams, results in a standing-wave component near the $z = 0$ plane. The complex-source/sink wave provides a rigorous solution to the wave equation in free-space over all space. In summary, the complex source/sink model, as opposed to the complex point-source model, yields an expression for the phasor of a physically realizable (singularity-free) beam.

Due to the partially standing-wave nature of such a solution, producing a complex-source/sink beam requires a focusing element that subtends a solid angle greater than 2π, such as a 4Pi microscope or the parabolic mirror of large extent schematically illustrated in Fig. 5. Qualitatively, it can be seen that incident rays on the parabolic mirror for which $r < r_0 = 2f$ contribute to the propagating beam, whereas rays for which $r > r_0$ contribute to the counter-propagating one, where f is the focal length of the parabolic mirror (Fig. 5). If the beam is focused by a focusing element that subtends a solid angle less than 2π, then the counter-propagating component of the beam cannot be produced physically. Nevertheless, in that case, the complex-source/sink solution can then be regarded as a rigorous solution to an approximate model.

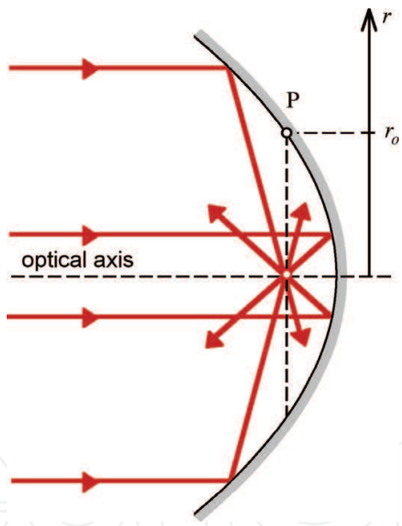

Fig. 5. Focusing a collimated beam with a parabolic mirror of large extent leads to propagating as well as counter-propagating contributions in the electromagnetic fields in the focal region of the mirror.

Higher-order nonparaxial Gaussian beams

The phasor of the fundamental nonparaxial Gaussian beam constitutes one among the infinite number of exact solutions to the Helmholtz equation. In fact, some of these additional solutions are the higher-order nonparaxial Gaussian modes. Shin and Felsen used the approach of Deschamps with a complex multipole source to produce higher-order beams that reduce to the elegant Hermite–Gaussian modes in the paraxial limit (Shin & Felsen, 1977). Phasors of nonparaxial beams, that may describe elegant higher-order beams

in cylindrical coordinates, were proposed by Couture and Bélanger. These phasors are expressed in terms of associated Legendre functions and spherical Hankel functions of complex arguments (Couture & Bélanger, 1981). Landesman and Barrett obtained the same solutions using the oblate spheroidal coordinates (Landesman & Barrett, 1988). Such phasors can be viewed as being generated with the complex point-source method, leading to nonphysically realizable beams.

Singularity-free phasors of higher-order nonparaxial beams can be generated with the help of the complex source/sink method. The higher-order nonparaxial beams proposed by Ulanowski and Ludlow are in turn expressed in terms of associated Legendre functions and spherical Bessel functions of the first kind (Ulasnowski & Ludlow, 2000):

$$\tilde{\psi}^{e}_{n,m}(r,\phi,z) = \exp(-ka)\, j_n(k\tilde{R})\, P_n^m(\cos\tilde{\theta})\cos(m\phi)\,, \tag{16}$$

where $\cos\tilde{\theta} \equiv (z+ja)/\tilde{R}$, $j_n(k\tilde{R})$ is the spherical Bessel function of the first kind of order n, and $P_n^m(\cos\tilde{\theta})$ is the associated Legendre function. Eq. (16) is an exact solution to the Helmholtz equation. Spherical Bessel functions in Eq. (16) are preferred to spherical Hankel functions suggested by Couture and Bélanger to ensure the absence of singularity in the plane of the beam waist ($z = 0$) at $r = a$. The explicit form of the fundamental mode ($n = m = 0$) in Eq. (16) is $\tilde{\psi}^{e}_{0,0} = \exp(-ka)\, j_0(k\tilde{R}) = \exp(-ka)\sin(k\tilde{R})/(k\tilde{R})$ and it is proportional to the singularity-free nonparaxial Gaussian beam [Eq. (15)], as expected.

While Shin and Felsen have shown that the complex point-source method leads to the elegant nonparaxial Hermite–Gaussian modes, Seshadri employed the method to find the differential and the integral representations of the nonparaxial cylindrically symmetric elegant Laguerre–Gaussian modes (Seshadri, 2002). Two years later, Bandres and Gutiérrez-Vega presented the same analysis without the restriction on the cylindrical symmetry, providing the complete differential and integral representations of the nonparaxial elegant Laguerre–Gaussian modes, denoted by $\tilde{U}^{\sigma}_{p,m}(\mathbf{r},\omega)$ where $\sigma = \{e,o\}$ is the parity (Bandres & Gutiérrez-Vega, 2004). However, these expressions exhibit the axial discontinuity as well as the circular singularity in the plane of the beam waist. Closed-form expressions for the phasor $\tilde{U}^{\sigma}_{p,m}(\mathbf{r},\omega)$ of the singularity-free nonparaxial elegant Laguerre–Gaussian beam can be written as a finite sum (April, 2008a):

$$\tilde{U}^{\sigma}_{p,m}(\mathbf{r},\omega) = F(\omega)2^{p+2}\left(\frac{ka}{2}\right)^{p+1+m/2}\sum_{s=0}^{p}\binom{p+m}{s+m}\frac{(4s+2m+1)(2s-1)!!}{(2p+2s+2m+1)!!}\tilde{\psi}^{\sigma}_{2s+m,m}(r,\phi,z)\,. \tag{17}$$

This particular linear combination of functions $\tilde{\psi}^{\sigma}_{n,m}(r,\phi,z)$, as given by Eq. (17), has the property to reduce to the elegant Laguerre–Gaussian beam defined by Eq. (5) in the paraxial limit. Actually, another function denoted by $\tilde{V}^{\sigma}_{p,m}(\mathbf{r},\omega)$ has the same property. Whereas $\tilde{U}^{\sigma}_{p,m}(\mathbf{r},\omega)$ is written as a linear combination of functions $\tilde{\psi}^{\sigma}_{n,m}(r,\phi,z)$ for which $n - m$ is even, $\tilde{V}^{\sigma}_{p,m}(\mathbf{r},\omega)$ is a linear combination of functions $\tilde{\psi}^{\sigma}_{n,m}(r,\phi,z)$ for which $n - m$ is odd:

$$\tilde{V}^{\sigma}_{p,m}(\mathbf{r},\omega) = -jF(\omega)2^{p+2}\left(\frac{ka}{2}\right)^{p+1+m/2}\sum_{s=0}^{p}\binom{p+m}{s+m}\frac{(4s+2m+3)(2s+1)!!}{(2p+2s+2m+3)!!}\tilde{\psi}^{\sigma}_{2s+m+1,m}(r,\phi,z)\,. \tag{18}$$

It is clear that $\tilde{U}^{\sigma}_{p,m}(\mathbf{r},\omega)$ and $\tilde{V}^{\sigma}_{p,m}(\mathbf{r},\omega)$ in Eqs. (17) and (18) are also exact solutions of the Helmholtz equation, because they are written as a linear combination of functions $\tilde{\psi}^{\sigma}_{n,m}(r,\phi,z)$, which are themselves rigorous solutions of the Helmholtz equation. In the paraxial limit ($ka >> 1$), both solutions reduce to the phasor of the paraxial elegant Laguerre–Gaussian beam (April, 2008a):

$$\lim_{ka>>1} \tilde{U}^{\sigma}_{p,m}(\mathbf{r},\omega) = \lim_{ka>>1} \tilde{V}^{\sigma}_{p,m}(\mathbf{r},\omega) = \tilde{u}^{\sigma}_{p,m}(\mathbf{r},\omega). \tag{19}$$

Both solutions $\tilde{U}^{\sigma}_{p,m}(\mathbf{r},\omega)$ and $\tilde{V}^{\sigma}_{p,m}(\mathbf{r},\omega)$ form a complete eigenfunction basis for the Helmholtz equation. These solutions are expressed as a simple linear combination of spherical Bessel functions and associated Legendre functions of complex arguments.

3.3 The Poisson-like spectrum

As mentioned in Section 2.3, the Gaussian spectrum is not appropriate to characterize arbitrarily short pulses, because it contains spectral components of appreciable amplitude with negative frequencies when the spectrum is broad enough. A suitable spectrum $F(\omega)$ whose spectral content does not extend in the negative frequencies must be chosen to adequately describe an ultrashort pulse. Here, we choose the Poisson-like spectral amplitude (also called the power spectrum), defined by (Caron & Potvliege, 1999; Feng & Winful, 2000)

$$F(\omega) = 2\pi \exp(j\phi_o)\left(\frac{s}{\omega_o}\right)^{s+1} \frac{\omega^s \exp\left(-s\omega/\omega_o\right)}{\Gamma(s+1)}\theta(\omega), \tag{20}$$

where s is a real positive parameter, ϕ_o is the absolute phase of the pulse, ω_o is the frequency for which the spectral amplitude is maximum, $\Gamma(\cdot)$ is the gamma function, and $\theta(\omega)$ is the unit step function which ensures that the pulse does not exhibit negative frequencies. This will make the time-domain complex fields analytic functions that are well behaved for all time and all points in space. Since $F(0) = 0$, it follows that the pulse does not have a dc component. The parameter s controls the shape and the width of the spectrum (Fig. 6a). Chirped pulses may be modeled by taking ω_o as a complex number.

Spectra of the form expressed in Eq. (20) are often observed in terahertz experiments and may also be used to describe femtosecond laser pulses. Moreover, spectra described by Eq. (20) lead to closed-form expressions for the electromagnetic fields of isodiffracting pulsed beams in terms of elementary functions. The inverse Fourier transform of Eq. (20) gives

$$f(t) \equiv \frac{1}{2\pi}\int_{-\infty}^{\infty} F(\omega)\exp(j\omega t)\mathrm{d}\omega = \exp(j\phi_o)\left(1 - \frac{j\omega_o t}{s}\right)^{-(s+1)} \tag{21}$$

The real part of $f(t)$ provides the temporal shape of the pulse. A pulse for which s is close to unity is a single-cycle pulse (Fig. 6b).

It can be shown that the spectral amplitude as well as the temporal shape of the pulse reduce to Gaussian functions in the limit of a narrow spectrum, i.e. when s is very large (Caron & Potvliege, 1999):

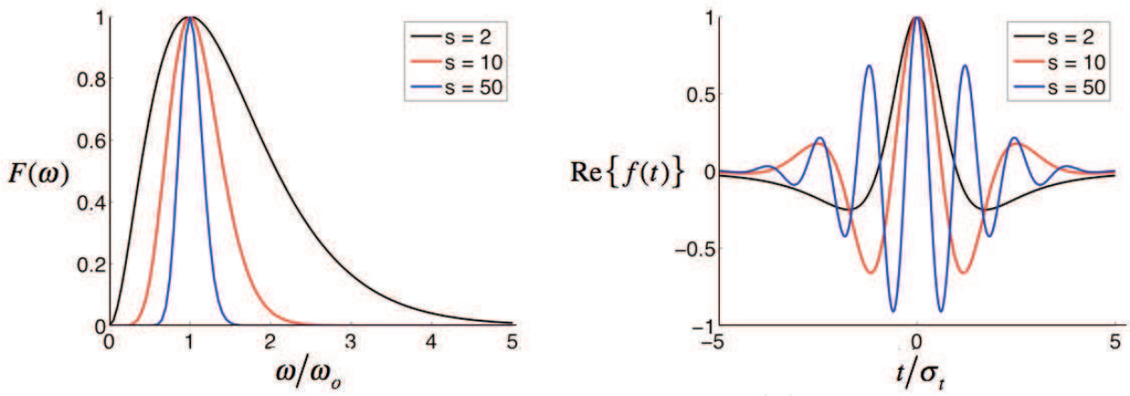

(a) (b)

Fig. 6. (a) Spectral and (b) temporal shape of the pulse for different values of parameter s, with a zero absolute phase ϕ_o.

$$F(\omega) \sim \sqrt{\pi} T \exp\left[-\tfrac{1}{4} T^2 (\omega - \omega_o)^2 + j\phi_o\right] \theta(\omega) \tag{22a}$$

and

$$f(t) \sim \exp\left[-\frac{t^2}{T^2} + j(\omega_o t + \phi_o)\right], \tag{22b}$$

if $s >> 1$, where $T \equiv (2s)^{1/2} / \omega_o$ is the duration of the Gaussian pulse. These results are coherent with the fact that the Fourier transform of a Gaussian function is also a Gaussian function. Thus, the Poisson-like spectrum is an interesting alternative to describe a pulse whose spectrum reduces to a Gaussian function if its duration is sufficiently long.

Hereafter, the parameter σ_t, defined as the root mean square (RMS) width of the temporal distribution $|f(t)|^2$, will be used as the expression of the pulse duration. Also, the RMS width σ_ω of the spectral intensity $|F(\omega)|^2$ will be employed to evaluate the width of the spectrum. Their expressions are explicitly

$$\sigma_t = \frac{1}{\omega_o} \frac{s}{(2s-1)^{1/2}}, \tag{23a}$$

$$\sigma_\omega = \frac{\omega_o}{2} \frac{(2s+1)^{1/2}}{s}. \tag{23b}$$

According to Eqs. (23a) and (23b), the inequality $\sigma_t \sigma_\omega \geq 1/2$ is verified as it must be for every pair of Fourier transforms; furthermore, $\sigma_t \sigma_\omega = 1/2$ in the limit $s \to \infty$, in which case the distributions become Gaussian functions.

4. Characterization of some laser pulses

Combining the Hertz potential method, the complex-source/sink model and the Poisson-like spectrum, it is possible to obtain the expressions for electromagnetic fields that are rigorous solutions to Maxwell's equations. In principle, any kind of pulsed beam can be

generated with this approach. In particular, transverse magnetic, transverse electric, and linearly polarized pulses will be analyzed. The isodiffracting pulse will then be discussed as an important special case.

4.1 Previous works on laser pulses

Many authors have studied models of pulsed beams, which are unfortunately incomplete or intricate. For instance, Kiolkowski and Judkins explored the simple case of a paraxial Gaussian pulsed beam, where they have considered that the waist spot size w_0 is the same for all the spectral components of the pulse (Kiolkowski & Judkins, 1992). As a consequence, they were not able to get a general analytical expression for their Gaussian pulsed beam applicable for all z; only results valid in the limiting cases of the far field ($z >> z_R$) and the near field ($z << z_R$) have been found. Wang *et al.* found in turn the expression of a paraxial Gaussian pulsed beam that satisfies the so-called isodiffracting condition, according to which the Rayleigh range z_R is the same for all spectral components (Wang *et al*., 1997). Thus, they obtained a general and remarkably simple closed-form expression for the Gaussian pulsed beam, only valid for paraxial beams and long enough pulses. A year later, Porras found the expression for an ultrafast Gaussian pulsed beam (Porras, 1998), shedding light on the spatiotemporal couplings that occur when a pulse propagates in free space (the diffractional effects depend on time and the temporal shape of the pulse depends on the spatial distribution of the pulse).

In the context of the complex point-source method, Heyman and Felsen determined the expression of a nonparaxial pulse, using the isodiffracting condition that, according to them, means that the confocal parameter a is frequency independent (Heyman & Felsen, 2001). It should be noted that, in the paraxial limit where $a \approx z_R$, this definition of the isodiffracting condition is equivalent to the one from Wang *et al*. With the help of the complex-source/sink model, Saari provided an expression for a scalar singularity-free nonparaxial pulse, written in terms of the oblate spheroidal coordinates (Saari, 2001).

The previously mentioned authors did not take into account the vector nature of their pulses. But Lu *et al.* presented the expressions for the electromagnetic fields of a nonparaxial pulsed beam; these expressions were obtained with a perturbative method and the results are expressed as a truncated series written in terms of convolutions (Lu *et al*., 2003). In principle, the method of Lax *et al*. is used in order to add spatial corrections to the paraxial beam. In 2006, Varin *et al*. succeeded in generalizing this method to the spatiotemporal corrections to the paraxial vector pulsed beam (Varin *et al*., 2006); using their approach, they have obtained the expression of a special nonparaxial ultrashort pulsed beam, expressed as an infinite series.

4.2 Some special pulses

The complex source/sink method yields a rigorous solution $\tilde{\Psi}(\mathbf{r},\omega)$ to the Helmholtz equation in the frequency domain, which represents a nonzero component of a Hertz potential. To describe a well-behaved pulse, the spectrum of $\tilde{\Psi}(\mathbf{r},\omega)$ is chosen so that it does not contain spectral components of negative frequency. The scalar field $\tilde{\Psi}(\mathbf{r},\omega)$ can be proportional to the nonparaxial Gaussian beam defined by Eq. (15). Otherwise, the nonparaxial elegant Laguerre–Gaussian beam $\tilde{U}^{\sigma}_{p,m}(\mathbf{r},\omega)$ may be used to describe higher-order beams. Once the solution for $\tilde{\Psi}(\mathbf{r},\omega)$ is known, the spatiotemporal component of the Hertz potential $\Psi(\mathbf{r},t)$ is recovered by taking its inverse Fourier transform (Fig. 1):

$$\Psi(\mathbf{r},t)=\frac{1}{2\pi}\int_{-\infty}^{\infty}\tilde{\Psi}(\mathbf{r},\omega)\exp(j\omega t)\mathrm{d}\omega\,. \tag{24}$$

For a given state of polarization, both electric and magnetic Hertz potentials can be constructed. Three states of polarization can easily be generated with the Hertz potential method: the transverse magnetic (TM), the transverse electric (TE), and the linearly polarized (LP) pulsed beams (Table 3).

TM pulsed beam	TE pulsed beam	LP pulsed beam in the x-direction
$\mathbf{\Pi}_e=\hat{\mathbf{a}}_z\Psi(\mathbf{r},t)$	$\mathbf{\Pi}_e=\mathbf{0}$	$\mathbf{\Pi}_e=\hat{\mathbf{a}}_x\Psi(\mathbf{r},t)$
$\mathbf{\Pi}_m=\mathbf{0}$	$\mathbf{\Pi}_m=\hat{\mathbf{a}}_z\eta_0^{-1}\Psi(\mathbf{r},t)$	$\mathbf{\Pi}_m=\hat{\mathbf{a}}_y\eta_0^{-1}\Psi(\mathbf{r},t)$

Table 3. Electric and magnetic Hertz potentials for TM, TE and LP pulsed beams.

Then, the expressions for the electromagnetic fields can be determined with the help of Eqs. (11a) and (11b). Since the spectrum of $\tilde{\Psi}(\mathbf{r},\omega)$ in Eq. (24) is one-sided, the resulting fields $\mathbf{E}(\mathbf{r},t)$ and $\mathbf{H}(\mathbf{r},t)$ are expressed in their complex analytical signal representations. The physical fields are simply obtained from the real part of $\mathbf{E}(\mathbf{r},t)$ and $\mathbf{H}(\mathbf{r},t)$. The lowest-order member of each family of pulsed beams listed in Table 3 is analyzed briefly in the following paragraphs.

The TM_{01} pulse

The TM_{01} beam is the lowest-order radially polarized beam. Therefore, the fundamental Gaussian beam ($p = m = 0$) must be chosen as the rigorous solution of the Helmholtz equation for the axial component of the electric Hertz potential. Since it is cylindrically symmetric, the function $\Psi(\mathbf{r},t)$ does not depend on the azimuthal angle ϕ, and Eqs. (11a) and (11b) can be simplified to give the nonzero cylindrical components of the electric and magnetic fields in terms of the electric Hertz potential (Table 4).

Electric field components		Magnetic field component
$E_r=\dfrac{\partial^2\Psi}{\partial z\partial r}$	$E_z=\dfrac{\partial^2\Psi}{\partial z^2}-\dfrac{1}{c^2}\dfrac{\partial^2\Psi}{\partial t^2}$	$H_\phi=-\varepsilon_0\dfrac{\partial^2\Psi}{\partial t\partial r}$

Table 4. The nonzero electromagnetic components of a TM_{01} pulsed beam.

A TM_{01} pulse is said to be radially polarized since the azimuthal component of the electric field is zero, i.e. $E_\phi=0$. Furthermore, the pulse is transverse magnetic (TM), because the magnetic field of the optical pulse does not have a longitudinal component, as opposed to its electric field. In the paraxial regime, the electric energy density (defined by $W\equiv\frac{1}{2}\varepsilon_0|\mathbf{E}|^2$) on the axis is small compared to its maximum value, giving to the beam a "doughnut" shape; in the nonparaxial regime, the longitudinal component of the electric field dominates the radial component, so that the electric energy density is maximum at the center of the beam. The longitudinal component of the electric field of a strongly focused TM_{01} pulse can be exploited for electron acceleration (Varin *et al*., 2005).

The TE_{01} pulse

The expressions for the electromagnetic components of a TE_{01} pulsed beam may be easily derived from those of a TM_{01} pulsed beam by means of the previously mentioned duality transformation $\mathbf{E} \to \eta_0 \mathbf{H}$ and $\mathbf{H} \to -\mathbf{E}/\eta_0$ (Table 5).

Electric field component	Magnetic field components	
$E_\phi = \frac{1}{c}\frac{\partial^2 \Psi}{\partial t \partial r}$	$H_r = \frac{1}{\eta_0}\frac{\partial^2 \Psi}{\partial z \partial r}$	$H_z = \frac{1}{\eta_0}\left(\frac{\partial^2 \Psi}{\partial z^2} - \frac{1}{c^2}\frac{\partial^2 \Psi}{\partial t^2}\right)$

Table 5. The nonzero electromagnetic components of a TE_{01} pulsed beam.

A TE_{01} pulse is a special case of the family of the azimuthally polarized pulses; in fact, the radial component of the electric field is zero. Also, the pulse is said to be transverse electric (TE), since the electric field of the pulse does not have a longitudinal component while the longitudinal component of its magnetic field is nonzero. This beam is characterized by a transverse electric energy density profile of doughnut shape, in both the paraxial and nonparaxial regimes. Hence, an azimuthally polarized pulsed beam always has a zero intensity at the center of its transverse intensity distribution. As a result, a TE_{01} pulsed beam may have interesting applications in stimulated emission depletion (STED) microscopy (Deng *et al*., 2007).

The LP_{01} pulse

A linearly polarized beam is produced by a combination of crossed electric and magnetic dipoles located at an imaginary distance, which is called a LP beam. (Sheppard & Saghafi, 1999a). Because the LP_{01} beam is the lowest-order member of the family of the linearly polarized beams, the nonparaxial Gaussian beam defined by Eq. (15) is chosen as the exact solution of the Helmholtz equation for the nonzero Cartesian components of the Hertz potentials. Applying Eqs. (11a) and (11b), the six electromagnetic components of a LP_{01} pulsed beam in the x-direction can be computed (Table 6).

Electric field components	Magnetic field components
$E_x = \frac{\partial^2 \Psi}{\partial x^2} - \frac{1}{c^2}\frac{\partial^2 \Psi}{\partial t^2} + \frac{1}{c}\frac{\partial^2 \Psi}{\partial t \partial z}$	$H_x = \frac{1}{\eta_0}\frac{\partial^2 \Psi}{\partial x \partial y}$
$E_y = \frac{\partial^2 \Psi}{\partial y \partial x}$	$H_y = \frac{1}{\eta_0}\left(\frac{\partial^2 \Psi}{\partial y^2} - \frac{1}{c^2}\frac{\partial^2 \Psi}{\partial t^2} + \frac{1}{c}\frac{\partial^2 \Psi}{\partial t \partial z}\right)$
$E_z = \frac{\partial^2 \Psi}{\partial z \partial x} - \frac{1}{c}\frac{\partial^2 \Psi}{\partial t \partial x}$	$H_z = \frac{1}{\eta_0}\left(\frac{\partial^2 \Psi}{\partial z \partial y} - \frac{1}{c}\frac{\partial^2 \Psi}{\partial t \partial y}\right)$

Table 6. The electromagnetic components of a LP_{01} pulsed beam.

In the paraxial regime, the x-component of the electric field and the y-component of the magnetic field of the LP_{01} pulsed beam dominate the other field components, and the energy density profile has a Gaussian shape (it is sometimes called a TEM_{00} pulsed beam). In the nonparaxial regime, the power transferred from the transverse components of the electric field of the LP_{01} pulsed beam to its longitudinal component increases as the value of ka

decreases; the longitudinal component of the electric field is not cylindrically symmetric and, as a consequence, the focal spot becomes asymmetrically deformed and elongated in the direction of the polarization (here, in the x-direction).

4.3 Isodiffracting pulses

For isodiffracting pulses, all the frequency components have the same wavefront radius of curvature (Melamed & Felsen, 1998). For each traveling beam $\exp(\pm jk\tilde{R})/\tilde{R}$ that constitutes the expression of Eq. (15), the wavefront is an oblate spheroid with a radius of curvature whose length is given by the real part $a\xi$ of the complex spherical radius $\tilde{R}$. It is seen from Eq. (13a) that ξ depends only on the spatial coordinates and on the parameter a. Therefore, the confocal parameter a of an isodiffracting pulse must be frequency independent (Heyman & Felsen, 2001). Note that, in the paraxial limit, it means that all the spectral components of an isodiffracting pulse have the same Rayleigh range z_R, as it is well known.

Closed-form expressions for the electromagnetic fields of an isodiffracting strongly focused, ultrafast laser pulse can be obtained. With the isodiffracting condition, the inverse Fourier transform of Eq. (15) can easily be carried out. If $f(t)$ is the inverse Fourier transform of $F(\omega)$, then substituting Eq. (15) in Eq. (24) and performing the integration yields

$$\Psi(\mathbf{r},t) = \frac{\Psi_o}{\tilde{R}}\left[f(\tilde{t}_+) - f(\tilde{t}_-)\right], \tag{25}$$

where $\Psi_o \equiv \tilde{\Psi}_o/2j$ is a constant amplitude, $\tilde{t}_\pm \equiv t \pm \tilde{R}/c + j\,a/c$, and c is the speed of light in vacuum. The time $t = 0$ corresponds to the instant for which the pulse is in the plane of the beam waist, which is located at $z = 0$. The introduction of the complex temporal variables $\tilde{t}_\pm$ in Eq. (25) shows that in general there is a spatiotemporal coupling. Moreover, Eq. (25) contains all the information about the spatial and temporal behaviors of the pulsed beam.

An understanding of the properties of isodiffracting pulses is particularly relevant for studying the spatiotemporal behavior of mode-locked laser pulses. As Eq. (25) shows, isodiffracting pulses have the advantage of being easily analyzed with simple closed-form expressions. However, if one has to characterize a nonisodiffracting pulsed beam (whose frequency components do not have all the same confocal parameter), the method presented in this chapter is still applicable, but a closed-form analytical solution may be not obtained; in general, numerical integrations have to be performed.

5. The isodiffracting TM_{01} pulsed beam

To explore the method proposed in this chapter, let us consider the TM_{01} mode-locked laser pulse. The TM_{01} beam in particular is analyzed in detail because of its practical importance comparatively to other TM, TE or LP beams. Quabis, Dorn and co-workers have shown that smaller spot sizes can be achieved with a radially polarized beam instead of a linearly polarized beam (Quabis *et al.*, 2000). Because of their remarkable focusing properties, TM_{01} beams are of considerable interest, for example, in high-resolution microscopy. Moreover, when it is strongly focused, the electric field of the TM_{01} pulsed beam has a significant longitudinal component that can be exploited in particle trapping and electron acceleration (Varin *et al.*, 2005). First, some techniques to generate TM_{01} beams are briefly discussed; second, the expressions of the electromagnetic fields of a TM_{01} pulsed beam are presented; then, the focusing properties of an isodiffraction TM_{01} pulse are briefly explored.

5.1 Generation of TM_{01} beams

The TM_{01} beam can be viewed as a coherent combination of two orthogonally polarized elegant Laguerre-Gaussian modes of order (0,1); the first mode is horizontally polarized and has a $\cos\phi$ angular dependence, where ϕ is the azimuthal angle, and the second mode is vertically polarized with a $\sin\phi$ azimuthal dependence (Fig. 7). The result of this superposition is radially polarized and its electromagnetic fields has transverse components that are proportional to elegant Laguerre–Gaussian modes of order (0,1).

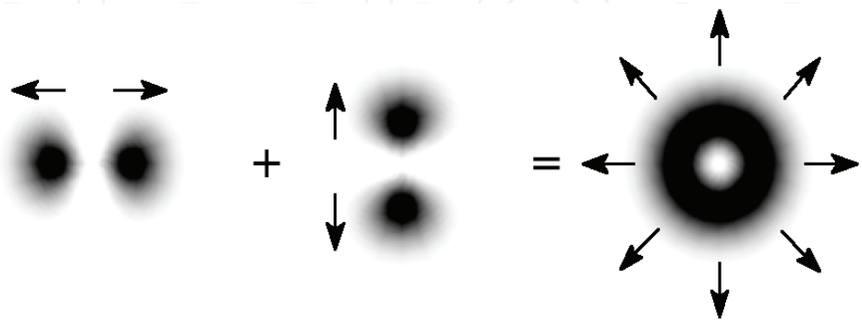

Fig. 7. A TM_{01} laser beam can be seen as a coherent superposition of two orthogonally polarized Laguerre-Gaussian modes of order (0,1). The arrows represent the spatial distribution of the instantaneous electric vector field.

Many approaches have been demonstrated to produce TM_{01} beams in laboratory. To name a few, a TM_{01} beam can be generated interferometrically, outside the resonator, with a Mach–Zehnder interferometer which allows the coherent superposition of two orthogonally polarized Laguerre–Gaussian beams of order (0,1) of different parity with the same beam waist (Tidwell *et al*., 1990). Radially polarized beams may be generated directly from a laser by inserting in the laser cavity axially-symmetric optical elements with suitable polarization selectivity; such elements include a conical reflector used as a resonator mirror, a conical Brewster window and a birefringent *c*-cut laser crystal (Kawauchi *et al*., 2008). Other techniques to produce pseudo-radially polarized beams involve, for instance, a polarization converter consisting in four half-wave plates, one in each quadrant (Dorn *et al*., 2003).

5.2 Electromagnetic fields of a nonparaxial TM_{01} pulsed beam

The analytical expressions for the electromagnetic fields can be obtained by computing the derivatives presented in Table 4 with Eq. (25):

$$E_r(\mathbf{r},t)=\frac{\Psi_o\sin(2\tilde{\theta})}{2\tilde{R}}\left[\frac{3}{\tilde{R}^2}\left(f(\tilde{t}_+)-f(\tilde{t}_-)\right)-\frac{3}{c\tilde{R}}\left(\frac{\partial f(\tilde{t}_+)}{\partial t}+\frac{\partial f(\tilde{t}_-)}{\partial t}\right)+\frac{1}{c^2}\left(\frac{\partial^2 f(\tilde{t}_+)}{\partial t^2}-\frac{\partial^2 f(\tilde{t}_-)}{\partial t^2}\right)\right] \quad (26)$$

$$E_z(\mathbf{r},t)=\frac{\Psi_o}{\tilde{R}}\left\{\frac{\left(3\cos^2\tilde{\theta}-1\right)}{\tilde{R}}\left[\frac{f(\tilde{t}_+)-f(\tilde{t}_-)}{\tilde{R}}-\frac{1}{c}\left(\frac{\partial f(\tilde{t}_+)}{\partial t}+\frac{\partial f(\tilde{t}_-)}{\partial t}\right)\right]-\frac{\sin^2\tilde{\theta}}{c^2}\left(\frac{\partial^2 f(\tilde{t}_+)}{\partial t^2}-\frac{\partial^2 f(\tilde{t}_-)}{\partial t^2}\right)\right\} \quad (27)$$

$$H_\phi(\mathbf{r},t)=\frac{\varepsilon_0\Psi_o\sin\tilde{\theta}}{\tilde{R}}\left[\frac{1}{\tilde{R}}\left(\frac{\partial f(\tilde{t}_+)}{\partial t}-\frac{\partial f(\tilde{t}_-)}{\partial t}\right)-\frac{1}{c}\left(\frac{\partial^2 f(\tilde{t}_+)}{\partial t^2}+\frac{\partial^2 f(\tilde{t}_-)}{\partial t^2}\right)\right], \quad (28)$$

where the complex angle $\tilde{\theta}$ is still defined such as $\cos\tilde{\theta} \equiv (z + ja)/\tilde{R}$. The resulting pulsed beam is isodiffracting in the sense that all the frequency components have the same confocal parameter *a*. It should be pointed out that the use of Eq. (20) as the spectral amplitude of the pulse is consistent with the net-force condition $\int_{-\infty}^{\infty} \mathbf{E}(\mathbf{r},t)\mathrm{d}t = \mathbf{0}$ that all laser pulses must satisfy (Milosevic *et al.*, 2006). Also, Eqs. (26)–(28) are consistent with the self-induced blueshift reported by Lin *et al.*, which implies that, for a ultrashort pulsed beam, the instantaneous frequency is highest at the center of the pulse and always higher than the carrier frequency ω_o (Lin *et al.*, 2006).

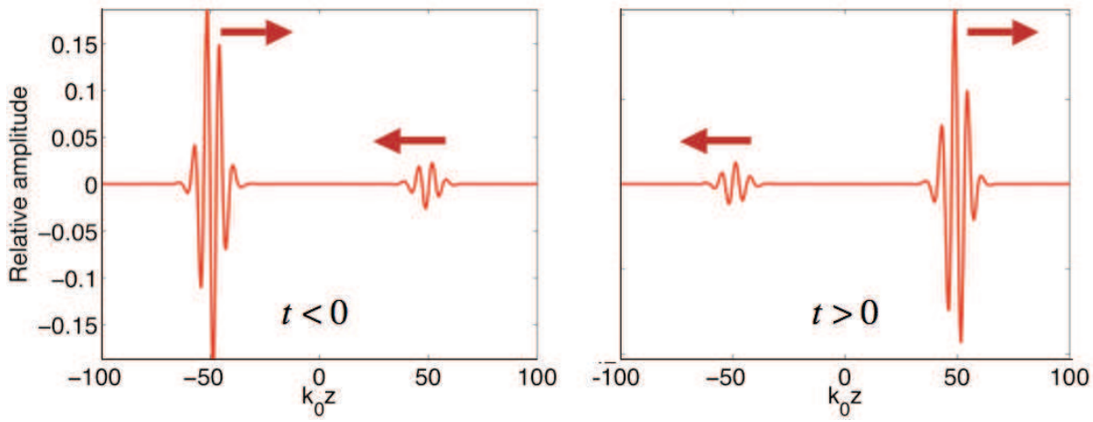

(a) (b)

Fig. 8. The numerical calculations of the on-axis (r = 0) propagation of the pulse described by the real part of Eq. (27), with $k_o a = \omega_o a/c = 2$, illustrate that the optical wave consists in the superposition of two counter-propagating pulses of different amplitudes.

It is apparent from Eqs. (26)–(28) that the electric field of the pulse is made of two contributions: the first one is due to terms involving $f(t)$ and its derivatives evaluated at $\tilde{t}_+$, and the second one to terms evaluated at $\tilde{t}_-$. In the case of the choice I for the value of $\tilde{R}$ [Eq. (14a)], the terms evaluated at $\tilde{t}_+$ describe two counter-propagating pulses of different amplitudes converging toward the plane of the beam waist (z = 0) for t < 0 and they vanish identically for t > 0. On the other hand, terms involving $\tilde{t}_-$ are zero for t < 0 whereas they represent the two counter-propagating pulses diverging from the plane of the beam waist for t > 0. In the case of the choice II for the value of $\tilde{R}$ [Eq. (14b)], the terms evaluated at $\tilde{t}_+$ describe a pulse traveling in the +z direction for all t, while terms involving $\tilde{t}_-$ represent a pulse of weaker amplitude traveling in the –z direction. In both case, the addition of these two contributions leads to Eqs. (26)–(28), which describe a strong purely traveling pulse superimposed to a counter-propagating traveling pulse of weaker amplitude for all t (Fig. 8). Such a field distribution certainly occurs when the nonparaxial pulse is generated by a 4π focusing system such as a parabolic mirror of large extent (see Fig. 5). Nonetheless, it can be verified that the amplitude of the counter-propagating pulse is very small compared to the amplitude of the propagating pulse even when the beam divergence angle is as large as 50°. Therefore, the amplitude of the counter-propagating pulse is negligible when the divergence angle of the pulsed beam is reasonably small.

The analytic signal (the complex-valued) electric field of the tightly focused, ultrafast TM_{01} pulse is obtained by using Eq. (21) in Eqs. (26)–(28). The expression of the physical electric

field is found by taking the real part of the resulting analytic signal. Some profiles of electric energy density, defined by $W(\mathbf{r},t)=\frac{1}{2}\varepsilon_0\left|\mathbf{E}(\mathbf{r},t)\right|^2$, of a TM_{01} pulse with different propagation parameters are shown in Fig. 9.

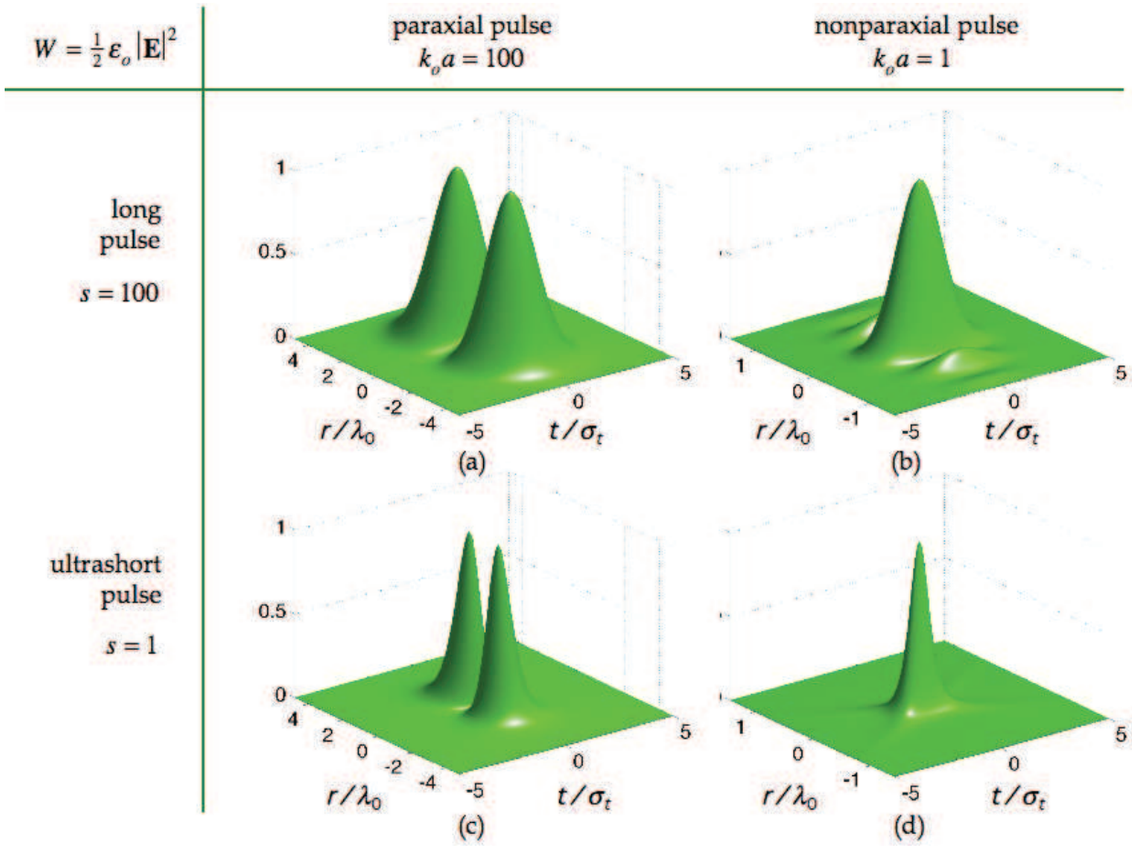

Fig. 9. The spatiotemporal shape of the electric energy density of a nonparaxial TM_{01} pulse is strongly dependent on the type of propagation regime.

It is instructive to compare the theoretical results to experimental data in order to validate the approach presented in this chapter. The intensity profile of a strongly focused TM_{01} pulsed beam has been obtained experimentally. The intensity distribution calculated numerically is in agreement with the experimental data (Fig. 10). For this experiment, a Ti:sapphire laser source emitting 140-fs pulses at 800 nm was used; this corresponds approximately to $\omega_o=2,4\times10^{15}$ rad/s and to $s=2\times10^5$. To produce the TM_{01} laser beam, a polarization converter was employed to convert a linearly polarized Gaussian beam into a radially polarized beam. Then, the pulsed beam was focused by a water immersion objective having a 1.2 numerical aperture, which corresponds to $k_o a=1$.

Very long pulses can be treated as continuous wave (CW) beams of frequency ω, for which the spectrum is infinitesimally narrow centered on the frequency ω. The spectrum of such a beam can be modeled by a Dirac delta centered on the frequency ω; the temporal shape of the beam reduces to $f(t)=\exp(j\omega t)$. Substituting this function in Eqs. (26)–(28) and computing the expressions of the electromagnetic fields of the nonparaxial TM_{01} beam, one can show that the results may be written as (Sheppard & Saghafi, 1999b; April, 2008b):

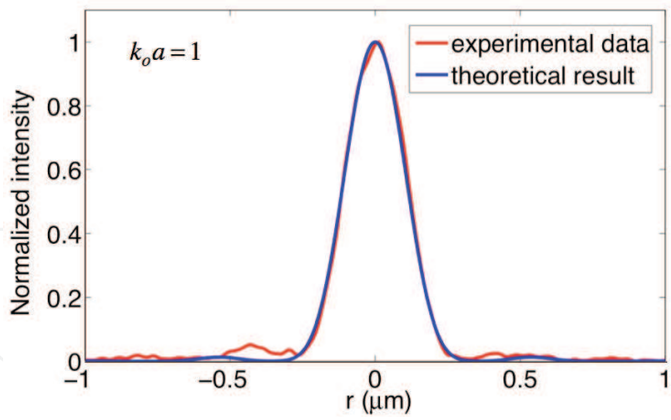

Fig. 10. The theoretical electric energy density profile in the beam waist is in agreement with the experimental data obtained with a Ti:Sapphire laser pulse for which $k_o a = 1$, $\omega_o = 2,4 \times 10^{15}$ rad/s and $s = 2 \times 10^5$. (Figure courtesy Harold Dehez, COPL, Université Laval)

$$E_r(\mathbf{r},t) = \tfrac{3}{4} E_o \exp(-ka + j\omega t) j_2(k\tilde{R}) \sin(2\tilde{\theta}), \tag{29}$$

$$E_z(\mathbf{r},t) = E_o \exp(-ka + j\omega t)\left[j_0(k\tilde{R}) + j_2(k\tilde{R}) P_2(\cos\tilde{\theta}) \right], \tag{30}$$

$$H_\phi(\mathbf{r},t) = j\tfrac{3}{2} H_o \exp(-ka + j\omega t) j_1(k\tilde{R}) \sin\tilde{\theta}, \tag{31}$$

where $E_o = \frac{4}{3} j\Psi_o k^3$ is a constant amplitude, $H_o = E_o/\eta_0$, $k = \omega/c$ is the wave number of the beam, $j_n(k\tilde{R})$ is the spherical Bessel function of the first kind of order n, and $P_2(\cos\tilde{\theta}) = \frac{1}{4}[1 + 3\cos(2\tilde{\theta})]$ is the Legendre polynomial of degree 2.

5.3 Focusing properties of isodiffracting TM_{01} pulses

The longitudinal component of the electric field of a TM_{01} beam is rotationally symmetric and exhibits an intensity distribution with a narrow central peak. When the TM_{01} beam is tightly focused, the contribution of the longitudinal component of its electric field dominates the contribution of the transverse components. Therefore, the electric energy density distribution in the plane of the beam waist is a sharp peak (Fig. 10). Moreover, it has been verified that the width of the electric density energy distribution of a TM_{01} beam is smaller than the one that could be obtained with a strongly focused LP_{01} beam (Quabis *et al.*, 2000).

The propagation of ultrashort pulses can differ significantly from that of the quasi-monochromatic light. In fact, the isodiffracting TM_{01} pulse exhibits interesting focusing properties: the width of its focal point becomes remarkably small as the duration of the pulse shortens (Fig. 11).

The full-width at half-maximum (FWHM) of the electric energy density of the nonparaxial TM_{01} pulse is $w_{\mathrm{FWHM}} = 0,401\lambda_o$ for the long pulse in Fig. 11a, where λ_o is the carrier wavelength, whereas it is $w_{\mathrm{FWHM}} = 0,145\lambda_o$ for the single-cycle pulse in Fig. 11c. Thus, according to this model, it appears that the radial extent of the pulse in the beam waist decreases as the pulse becomes shorter. Isodiffracting, tightly focused, ultrafast TM_{01} pulses turn out to have interesting focusing properties that may be exploited for superresolution and may have potential applications in high-resolution microscopy.

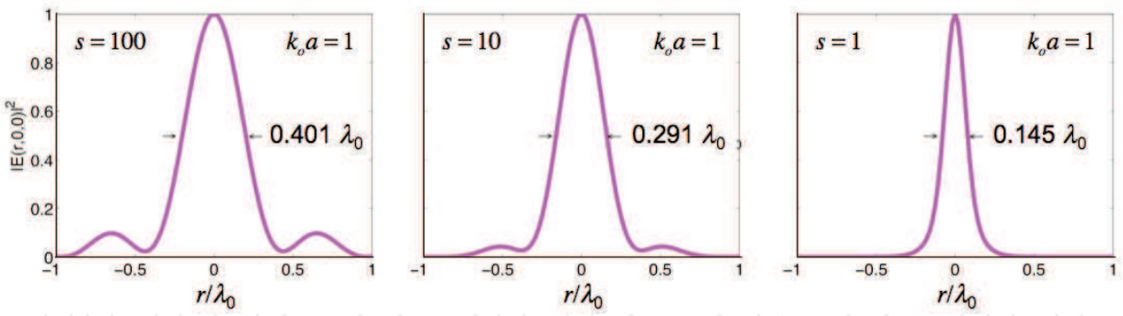

Fig. 11. As the pulse duration decreases (i.e. as s decreases), the width of the electric energy density profile of a tightly focused TM_{01} pulse with $k_o a = 1$ (i.e. a beam divergence angle of approximately 66°) in the plane of the beam waist ($z = 0$) decreases.

6. Conclusion

To conclude, we have presented a procedure to find the expressions for the electromagnetic fields of ultrashort, nonparaxial electromagnetic pulses that are rigorous solutions of the wave equation. The three main ingredients to build such solutions are (1) the Hertz potential method used to efficiently find an exact solution to Maxwell's four equations, (2) the complex-source/sink model employed to determine exact solutions to the Helmholtz equation that can be seen as the nonparaxial generalizations of the fundamental Gaussian beam and the higher-order Gaussian modes, and (3) the Poisson-like spectral amplitude of the form $\omega^s \exp(-s\omega/\omega_o)$ that allows the description of ultrafast pulses whose duration could be as short as one optical cycle. The analytical expressions for the electromagnetic fields found with this approach may be employed to investigate the spatiotemporal behavior of tightly focused, ultrafast laser pulses in free space.

As a continuation of this work, the treatment of nonisodiffracting pulses could be explored as well as the detailed study of higher-order pulsed beams. Finally, it would be interesting to extend the work presented in this chapter to the propagation of strongly focused, ultrashort pulses in a dispersive and/or nonlinear medium.

7. Acknowledgements

This work was supported by grants from Natural Sciences and Engineering Research Council of Canada (NSERC), the Fonds de recherche sur la nature et les technologies (FQRNT), Québec, the Canadian Institute for Photonic Innovations (ICIP/CIPI), and the Centre d'optique, photonique et lasers (COPL), Québec. The author thanks Michel Piché for helpful discussions and Harold Dehez for his contribution for the experimental data.

8. References

An der Brügge, D. & Pukhov, A. (2009). Ultrashort focused electromagnetic pulses. *Physical Review E,* Vol. 79, (January 2009) pp. 016603-1–016603-5, ISSN 1539-3755.

April, A. (2008a). Nonparaxial elegant Laguerre–Gaussian beams. *Optics Letters,* Vol. 33, No. 12, (June 2008) pp. 1392–1394, ISSN 0146-9592.

April, A. (2008b). Nonparaxial TM and TE beams in free space. *Optics Letters,* Vol. 33, No. 14, (July 2008) pp. 1563–1565, ISSN 0146-9592.

Bandres, M. A. & Gutiérrez-Vega, J. C. (2004). Higher-order complex source for elegant Laguerre–Gaussian waves. *Optics Letters,* Vol. 29, No. 19, (October 2004) pp. 2213–2215, ISSN 0146-9592.

Berardi, C.; Erricolo, D. & Uslenghi, P. L. E. (2004). Exact Dipole Radiation for an Oblate Spheroidal Cavity Filled With Isorefractive Material and Aperture-Coupled to a Half Space. *IEEE Transactions on Antennas and Propagation,* Vol. 52, No. 9, (September 2004) pp. 2205–2213, ISSN 0018-926X.

Caron, C. F. R. & Potvliege, R. M. (1999). Free-space propagation of ultrashort pulses: space-time couplings in Gaussian pulse beams. *Journal of Modern Optics,* Vol. 46, No. 13, (1999) pp. 1881–1891, ISSN 0950-0340.

Couture, M. & Bélanger, P.-A. (1981). From Gaussian beam to complex-source-point spherical wave. *Physical Review A,* Vol. 24, No. 1, (July 1981) pp. 355–359.

Deng, S. ; Liu, L. ; Li, R. & Xu, Z. (2007). STED microscopy with the azimuthally-polarized depletion beam, *Proceedings of SPIE*, Vol. 6826, pp. 682621-1-682621-7, Beijing, China, November 2007, SPIE.

Deschamps, G. A. (1971). Gaussian beam as a bundle of complex rays. *Electronics Letters,* Vol. 7, No. 23, (November 1971) pp. 684–685.

Dorn, R.; Quabis, S. & Leuchs, G. (2003). Sharper Focus for a Radially Polarized Light Beam. *Physical Review Letters,* Vol. 91, No. 23, (December 2003) pp. 233901-1–233901-4, ISSN 0031-9007.

Feng, S. & Winful, H. G. (2000). Spatiotemporal structure of isodiffracting ultrashort electromagnetic pulses. *Physical Review E,* Vol. 61, No. 1, (January 2000) pp. 862–873, ISSN 1063-651X.

Heyman, E. & Felsen L. B. (2001). Gaussian beam and pulsed-beam dynamics: complex-source and complex-spectrum formulations within and beyond paraxial asymptotics. *Journal of the Optical Society of America A,* Vol. 18, No. 7, (July 2001) pp. 1588–1611, ISSN 1084-7529.

Kawauchi, H; Kozawa, Y. & Sato, S. (2008). Generation of radially polarized Ti:sapphire laser beam using a c-cut crystal. *Optics Letters,* Vol. 33, No. 17, (September 2008) pp. 1984–1986, ISSN 0146-9592.

Landesman, B. T. & Barrett, H. H. (1988). Gaussian amplitude functions that are exact solutions to the scalar Helmholtz equation. *Journal of the Optical Society of America A,* Vol. 5, No. 10, (October 1988) pp. 1610–1619, ISSN 0740-3232.

Lax, M.; Louisell, W. H. & McKnight, W. B. (1975). From Maxwell to paraxial wave optics. *Physical Review A,* Vol. 11, No. 4, (April 1975) pp. 1365–1370.

Lin, Q.; Zheng, J. & Becker, W. (2006). Subcycle pulsed focused vector beams. *Physical Review Letters,* Vol. 97, (December 2006) pp. 253902-1–253902-4, ISSN 0031-9007.

Lu, G.; Guo, H.; Deng, D.; Yi, F. & Kong, H. J. (2003). Nonparaxially corrected solution for isodiffracting sub-cycle pulsed-beam propagation in free space. *Journal of the Korean Physical Society,* Vol. 42, No. 5, (May 2003) pp. 627–630, ISSN 0374-4884.

Melamed, T. & Felsen, L. B. (1998). Pulsed-beam propagation in lossless dispersive media. I. Theory. *Journal of the Optical Society of America A,* Vol. 15, No. 5, (May 1998) pp. 1268–1276, ISSN 0740-3232.

Milosevic, D. B.; Paulus, G. G.; Bauer, D. & Becker, W. (2006). Above-threshold ionization by few-cycle pulses. *Journal of Physics B: Atomic, Molecular and Optical Physics,* Vol. 39, No. 5, (July 2006) pp. R203–R262, ISSN 0953-4075.

Porras, M. A. (1998). Ultrashort pulsed Gaussian light beams. *Physical Review E,* Vol. 58, No. 1, (July 1998) pp. 1086–1093, ISSN 1063-651X.

Quabis, S.; Dorn, R.; Eberler, M.; Glöckl, O. & Leuchs G. (2000). Focusing light to a tighter spot. *Optics Communications,* Vol. 179, (May 2000) pp. 1–7, ISSN 0030-4018.

Richards, B. & Wolf, E. (1959). Electromagnetic diffraction in optical systems. II. Structure of the image field in an aplanatic system. *Proceedings of the Royal Society of London. Series A, Mathematical and Physical Sciences*, Vol. 253, No. 1274, (December 1959) pp. 358–379.

Rodríguez-Morales, G. & Chávez-Cerda, S. (2004). Exact nonparaxial beams of the scalar Helmholtz equation. *Optics Letters,* Vol. 29, No. 5, (March 2004) pp. 430–432, ISSN 0146-9592.

Saari, P. (2001). Evolution of subcycle pulses in nonparaxial Gaussian beams. *Optics Express,* Vol. 8, No. 11, (May 2001) pp. 590–598, ISSN 1094-4087.

Seshadri, S. R. (2002). Virtual source for a Laguerre–Gauss beam. *Optics Letters,* Vol. 27, No. 21, (November 2002) pp. 1872–1874, ISSN 0146-9592.

Sheppard, C. J. R. & Saghafi, S. (1998). Beam modes beyond the paraxial approximation: A scalar treatment. *Physical Review A,* Vol. 57, No. 4, (April 1998) pp. 2971–2979, ISSN 1050-2947.

Sheppard, C. J. R. & Saghafi, S. (1999a). Electromagnetic Gaussian beams beyond the paraxial approximation. *Journal of the Optical Society of America A,* Vol. 16, No. 6, (June 1999) pp. 1381–1386, ISSN 0740-3232.

Sheppard, C. J. R. & Saghafi, S. (1999b). Transverse-electric and transverse-magnetic beam modes beyond the paraxial approximation. *Optics Letters,* Vol. 24, No. 22, (November 1999) pp. 1543–1545, ISSN 0146-9592.

Sheppard, C. J. R. (2000). Polarization of almost-plane waves. *Journal of the Optical Society of America A,* Vol. 17, No. 2, (February 2000) pp. 335–341, ISSN 0740-3232.

Shin, S. Y.; Felsen, L. B. (1977). Gaussian beam modes by multipoles with complex source points. *Journal of the Optical Society of America,* Vol. 67, No. 5, (May 1977) pp. 699–700.

Siegman, A. E. (1986). *Lasers,* University Science Books, ISBN 0-935702-11-3, Sausalito, CA.

Tidwell, S. C.; Ford, D. H. & Kimura, W. D. (1990). Generating radially polarized beams interferometrically. *Applied Optics,* Vol. 29, No. 15, (May 1990) pp. 2234–2239, ISSN 0003-6935.

Ulanowski, Z. & Ludlow, I. K. (2000). Scalar field of nonparaxial Gaussian beams. *Optics Letters,* Vol. 25, No. 24, (December 2000) pp. 1792–1794, ISSN 0146-9592.

Varin, C.; Piché, M. & Porras, M. A. (2005). Acceleration of electrons from rest to GeV energies by ultrashort transverse magnetic laser pulses in free space. *Physical Review E,* Vol. 71, (February 2005) pp. 026603-1–026603-10, ISSN 1539-3755.

Varin, C.; Piché, M. & Porras, M. A. (2006). Analytical calculation of the longitudinal electric field resulting from the tight focusing of an ultrafast transverse-magnetic laser beam. *Journal of the Optical Society of America A,* Vol. 23, No. 8, (August 2006) pp. 2027–2038, ISSN 1084-7529.

Wang, Z.; Zhang, Z.; Xu, Z. & Lin, Q. (1997). Space–time profiles of an ultrashort pulsed Gaussian beam. *IEEE Journal of Quantum Electronics,* Vol. 33, No. 4, (April 1997) pp. 566–573, ISSN 0018-9197.

Ziolkowski, R. W. & Judkins, J. B. (1992). Propagation characteristics of ultrawide-bandwidth pulsed Gaussian beams. *Journal of the Optical Society of America A,* Vol. 9, No. 11, (November 1992) pp. 2021–2030, ISSN 0740-3232.

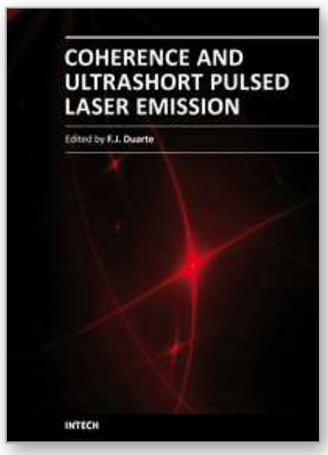

Coherence and Ultrashort Pulse Laser Emission

Edited by Dr. F. J. Duarte

ISBN 978-953-307-242-5
Hard cover, 688 pages
Publisher InTech
Published online 30, November, 2010
Published in print edition November, 2010

In this volume, recent contributions on coherence provide a useful perspective on the diversity of various coherent sources of emission and coherent related phenomena of current interest. These papers provide a preamble for a larger collection of contributions on ultrashort pulse laser generation and ultrashort pulse laser phenomena. Papers on ultrashort pulse phenomena include works on few cycle pulses, high-power generation, propagation in various media, to various applications of current interest. Undoubtedly, Coherence and Ultrashort Pulse Emission offers a rich and practical perspective on this rapidly evolving field.

How to reference

In order to correctly reference this scholarly work, feel free to copy and paste the following:

Alexandre April (2010). Ultrashort, Strongly Focused Laser Pulses in Free Space, Coherence and Ultrashort Pulse Laser Emission, Dr. F. J. Duarte (Ed.), ISBN: 978-953-307-242-5, InTech, Available from: http://www.intechopen.com/books/coherence-and-ultrashort-pulse-laser-emission/ultrashort-strongly-focused-laser-pulses-in-free-space

INTECH
open science | open minds

InTech Europe
University Campus STeP Ri
Slavka Krautzeka 83/A
51000 Rijeka, Croatia
Phone: +385 (51) 770 447
Fax: +385 (51) 686 166
www.intechopen.com

InTech China
Unit 405, Office Block, Hotel Equatorial Shanghai
No.65, Yan An Road (West), Shanghai, 200040, China
中国上海市延安西路65号上海国际贵都大饭店办公楼405单元
Phone: +86-21-62489820
Fax: +86-21-62489821

IntechOpen